Polymer 215 (2021) 123411

Contents lists available at ScienceDirect

Polymer

journal homepage: http://www.elsevier.com/locate/polymer

Time-resolving small angle X-Ray scattering analysis of melt crystallization of mixtures of regular and irregular isotactic polypropylene samples

Finizia Auriemma [a,*], Odda Ruiz de Ballesteros [a], Giovangiuseppe Giusto [b], Rocco Di Girolamo [a], Anna Malafronte [a], Miriam Scoti [a], Claudio De Rosa [a], Geoffrey R. Mitchell [c]

[a] Dipartimento di Scienze Chimiche, Università di Napoli "Federico II", Via Cintia, 80126, Napoli, Italy
[b] CIRA Italian Aerospace Research Centre, Via Maiorise, 81043, Capua (CE), IT, Italy
[c] Polytechnic Leiria, Centro Empresarial da Marinha Grande, Rua de Portugal - Zona Industrial, 2430 - 028, Marinha Grande, Portugal

ARTICLE INFO

Keywords:
Tactic polymer blends
Crystalline polymers
Phase separation
Melt strength

ABSTRACT

The melting/crystallization properties of blends obtained by mixing two isotactic polypropylene (iPP) samples synthesized using single-site metallocene catalyst systems and containing a high and low concentration of *rr* triads as stereo-defects, are studied. The changes occurring at lamellar length scale during a heating/cooling cycle at constant scanning rate are followed in situ by performing time-resolved small angle X-ray scattering (SAXS) measurements. Data analysis demonstrates that the evolution of the SAXS intensity with increase/decrease of the temperature is controlled by the separate melting/crystallization of the two components, the differences in the thermal expansion (contraction) coefficient of the amorphous and crystalline phases and the role of thermal fluctuations in electron density. The two components give rise to different populations of intermixed lamellar stacks in the blends which originate from the good miscibility of the low and high stereoregular samples in the melt.

1. Introduction

Vinyl polymers including a uniform distribution of stereo-defects may be considered as pseudo-copolymers characterized by only one type of monomers for which the configurational units approach a nearly random sequential distribution [1]. The structure-properties relationships of mixtures of pseudo-copolymers differing only for the configurational sequences of a given monomeric unit were studied for numerous couples of vinyl polymers characterized by a different kind and/or degree of stereoregularity [2–15], such as mixtures of vinyl polymers of different tacticity, or tactic polymers with different degree of stereoregularity [16–19]. As an example of the latter case of blends, a highly stereoregular isotactic iPP [16,17] or syndiotactic sPP [18,19] polypropylene sample of high melting temperature was mixed with a low stereoregular iPP and sPP sample, respectively, characterized by a low melting temperature. All blends show the separate melting and crystallization of the components, accelerated crystallization of the low stereoregular component, and intermediate mechanical properties between those of the pure samples. In particular, by mixing the two iPP samples, properties of highly crystalline, rigid thermoplastic materials are achieved at high concentration of the highly stereoregular component, gradually approaching elastomeric properties of low crystalline but still strong materials with increasing the concentration of the low stereoregular component [17]. Analogously, the blends obtained by mixing the sPP samples show high crystallinity, elastomeric properties and high rigidity typical of highly stereoregular sPP [20–33] at elevated concentration of the high stereoregular sample and gradually approach properties of low crystalline, thermoplastic elastomers with low modulus, with increasing the concentration of the low stereoregular sPP [19]. In both cases, the continuous change of mechanical properties of the blends with the concentration of the components was demonstrated to be similar to that one of stereo-irregular iPP [17] or sPP [19] samples having concentration of stereo-defects identical to the average concentration of stereo-defects in the blends [34,35]. As the concentration and type of stereo-defects in iPP and sPP is controlled in the synthetic step [36–41], the approach of blending two (isotactic or syndiotactic) pseudo-copolymers prepared with metallocene catalysts differing only for the concentration of stereo-defects was demonstrated to bring advantages compared to the use of a single iPP or sPP component with tailored concentration of stereo-defects, as a wide range of properties

* Corresponding author.
E-mail address: finizia.auriemma@unina.it (F. Auriemma).

https://doi.org/10.1016/j.polymer.2021.123411
Received 4 November 2020; Received in revised form 30 December 2020; Accepted 8 January 2021
Available online 13 January 2021

may be accessed using only two catalysts instead of resorting to a different metallocene catalyst for each targeted property [42–45]. All in all, the analysis suggests the hypothesis that the high and low stereoregular components establish good interactions in the melt and amorphous state.

Furthermore, for the iPP blends, a detailed analysis of the small angle X-ray scattering (SAXS) data of melt crystallized specimens indicated the tendency of the low and high stereoregular samples to form mixed lamellar stacks, in which the lamellar crystals are separated by amorphous layers including intermixed chains of the two components [16]. More precisely, upon cooling the melt, two leading populations of mixed lamellar crystals are formed, the relative amount of which depends on the blend composition. A first population of lamellar stacks consists of a dominant concentration of lamellar crystals from the highly stereoregular sample crystallizing at high temperature and includes in the interlamellar regions up to ≈30% of lamellae from the low stereoregular component crystallizing at lower temperature. The second main population of lamellar stacks is formed at low temperatures and includes the excess of the low stereoregular component, along with lamellar crystals of the highly stereoregular component not comprised in the first population.

The SAXS measurements of Ref. 16 were performed exclusively at room temperature on ex-situ melt-crystallized samples. In this manuscript, the changes occurring at lamellar length scale during the melting/crystallization processes of the isotactic pseudo-copolymers blends investigated in Ref. 16 and 17 is followed in situ by performing SAXS measurements. In particular, SAXS measurements are collected on samples during heating/cooling cycles at constant rate, and the analysis is extended also to the melt. As the two neat components show different melting and crystallization temperatures, the in situ analysis allows for investigating the structural changes involved in the separated processes.

Use of scattering methods for probing inhomogeneities in the melt of polymer blends due to thermal composition fluctuations is common [46–51]. This analysis is generally performed resorting to small angle neutron scattering experiments (SANS). Neutrons have the particularly important advantages of strong scattering contrast and deep penetration into materials, provided that a suitable blend component is totally or partially deuterated [51–53]. With use of SANS the phase diagrams for a variety of polymer blends have been determined in detail and a conclusive level of basic understanding has been achieved in this field [49–51]. In particular, the role of concentration fluctuations on phase separation at the critical points have been understood in terms of general theory of critical phenomena [47,49–51]. However, the SANS approach is limited due to the necessity of using deuterated samples especially in the case of polyolefins based samples, owing to the low contrast of scattering density length between the two components. Here, small angle X-ray scattering (SAXS) is demonstrated to be a valuable tool to study the melting/crystallization process of polyolefin blends, featuring only a low contrast in scattering density length between the two components.

2. Experimental

The blends are obtained by mixing two highly regio-regular, but stereo-defective iPP samples containing a uniform concentration of isolated *rr* triads equal to 0.49 (iPP-LS) and 9.53 mol% (iPP-HS), and nearly identical molecular masses (M_v (iPP-LS) = 196 kg/mol, M_v (iPP-HS) = 162 kg/mol),[16,17] where the codes "LS" and "HS" stand for low and high stereoregular samples, respectively. Both samples are crystalline and show melting temperatures of 162 °C for the sample iPP-HS and a double melting peak at 88 and 55 °C for the sample iPP-LS, whereas the crystallization temperatures are 117 and 32 °C, respectively [16,17].

Mixtures of iPP-HS/iPP-LS with composition 10/90, 30/70, 50/50, 70/30 and 90/10 by weight were prepared by dissolving the components in boiling xylene under reflux up to complete dissolution and successive precipitation with an excess of cold methanol containing 1 wt % of 2,6-di-*tert*-butyl-4-methylphenol as anti-oxidant. The weight loss of the filtered and successively (60 °C, 1 day) vacuum dried powders was less than 1 wt%. The samples were successively melted up to 210 °C in between the plates of a hydraulic press, kept at this temperature for 5 min, cooled down at room temperature by leaving the samples in between the press plates, and then finely ground in a mortar.

In agreement with ref. 17, wide angle X-ray scattering measurements (WAXS, Ni filtered Cu Kα radiation, Philips diffractometer) indicate that the iPP-HS/iPP-LS blends crystallize as mixtures of α form, due to the most crystalline component iPP-HS, and α/γ disordered forms, due to the less crystalline component iPP-LS (data not shown). The crystallization of α form is prevalent in blends with iPP-HS content higher than or equal to 30%, whereas, in blends with lower iPP-HS content, the crystallization of α/γ disordered forms becomes prevalent [17].

DSC thermograms, were recorded using Mettler-DSC30/2285 apparatus in flowing N_2 atmosphere at rate of 10 °C/min (Fig. S3).

SAXS data were collected at the beam line 2.1 of the Synchrotron Radiation Source in Daresbury (Cheshire, UK) (λ = 1.54 Å) at a sample to detector distance of 4 m on the melt crystallized and ground samples introduced in a borosilicate capillary. Data collection was performed using a Daresbury 2-D gas filled multiwire proportional detector with 512 × 512 pixels. Up to 255 frames could be stored in high speed memory using a programmable time sequence. The intensity digitization resolution was 16 bits. The pixel size to sample-detector length ratio was calibrated using the scattering recorded using collagen sample from a rat tail tendon. Time resolving measurements were performed during a heating run from 25 to 210 °C at a rate of 20 °C/min, followed by a 300 s isotherm at 210 °C and a successive cooling run at 10 °C/min. Data were collected every 10 s, on samples aged for at least two weeks. Subtraction for the empty sample holder and successive reduction and processing of the SAXS data were performed with the home-made program XESA [54]. A residual background (I_{back}) was also conventionally evaluated by fitting the tails of the SAXS curves (q range 1.4–1.8 nm^{-1}) with the relationship, ($Pq^{-n} + I_{back}$), by setting n = 4 where P is a fitting parameter proportional to the Porod constant.

Polarized optical microscopy (POM) images were recorded with an "Axioskop 40" optical microscope by Zeiss equipped with a Mettler FP90 central processor coupled with a FP82 HT heating/freezing stage. A small amount of solution precipitated samples sandwiched between two glass slides were melted at 180 °C, kept for 10 min at this temperature and then cooled to room temperature in air, to obtain transparent films having a smooth surface and uniform thickness of about 30–50 μm. The resultant films were then placed in the heating/freezing stage, heated up to 200 °C and, after a 10 min isotherm at this temperature, cooled down to room temperature at a rate of 1 °C/min, while recording POM images.

3. Results and discussion

3.1. Melting and crystallization analysis

The Lorentz corrected SAXS profiles of the iPP-HS/iPP-LS blends at 10/90, 50/50 and 90/10 composition are reported in Fig. 1 as an example. The corresponding SAXS profiles before the Lorentz correction are reported in Fig. S1. They are collected during a heating run at 20 °C/min, and the successive cooling at 10 °C/min. All curves show only a single correlation peak. The position q_{max} of the maximum in the correlation peaks and the corresponding intensity values I_{max} are reported in Fig. 2 and S2 as a function of the temperature.

It is worth noting that with the sole exception of the blend iPP-HS/iPP-LS 10/90 (Fig. 1A,A′), the correlation peaks tend to become stronger and sharper with increasing the temperature, during the heating, and weaker and broader with the decrease of the temperature, during the successive cooling (Fig. 1B,B′,C,C′). On the opposite, for the iPP-LS rich blend 10/90 (Fig. 1A,A′), the sharpness and strength of the correlation peak decrease with increase of the temperature (Fig. 1A) and increase with decrease of the temperature (Fig. 1A'). Furthermore, for

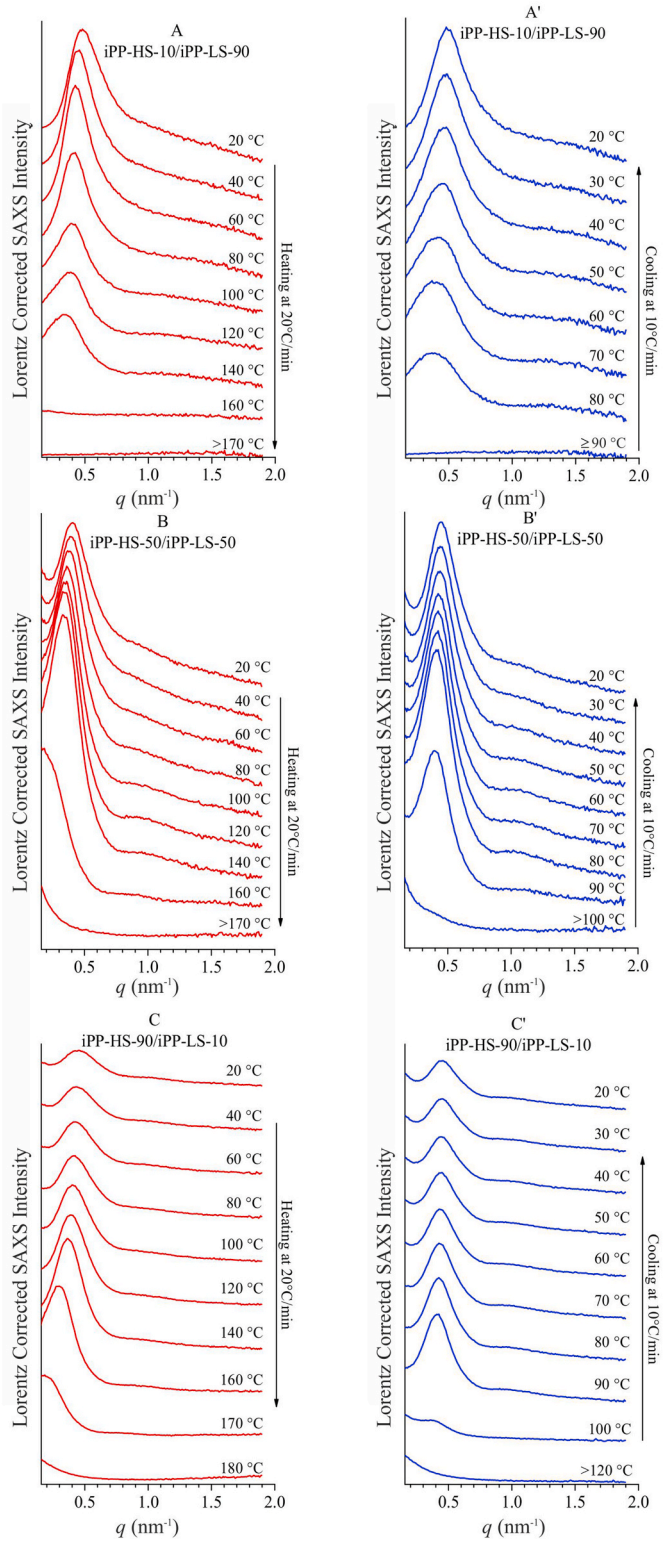

Fig. 1. Lorentz corrected SAXS intensity of iPP-HS/iPP-LS blends at composition 10/90 (A,A′), 50/50 (B,B′) and 90/10 (C/C′) recorded in situ during the heating step at 20 °C/min (A–C) and the successive cooling step at 10 °C/min (A′-C′).

all blends, the position of the maximum (q_{max}) tends to shift toward lower q values with increase of the temperature, during the heating and toward higher q values, with decrease of the temperature during the cooling (Fig. 2A–C and S2A). Simultaneously, the corresponding intensity values I_{max} (Fig. 2A'-C′ and S2A') tend to increase (decrease) with increase (decrease) of the temperature, while showing stepwise changes in the shape of more or less pronounced undulations.

The shift of q_{max} indicates that the average interlamellar distance L ($=2\pi/q_{max}$) increases (decreases) during the heating (cooling) by about 3–5% before melting (during crystallization). These changes are only in part due to the thermal expansion (contraction) of the average interlamellar distance, as they are also caused by the gradual melting (crystallization) of the low stereoregular component which, as demonstrated in Ref. 16, forms imperfect and thin lamellar crystals located in the interlamellar regions of the highly stereoregular component. It is worth noting that a possible contribution to the increase of the average lamellar distance due to lamellar thickening of the highly stereoregular component iPP-HS possibly occurring through chain sliding diffusion mechanisms [55–57] and/or melting-recrystallization phenomena may be ruled out, as, compared with the time lapse involved at the adopted heating rate of 20 °C/min, chain sliding [55–57] and melting/-recrystallization would be too slow. On the other hand, in the low temperature range, although melting/recrystallization phenomena for the low stereoregular component iPP-LS are feasible (*vide infra*), the consequent lamellar thickening would have only a scarce effect on the values of the average interlamellar distances.

The concomitant low temperature undulations of I_{max}, at about 80 °C during heating (≈50 °C during cooling) occur in correspondence of the melting (crystallization) of the low stereoregular component, whereas the high temperature drops (rises) of the I_{max} values at about 150–160 during heating (≈90–100 during cooling) mark the final melting (initial crystallization) of the highly stereoregular component, in agreement with the results of the DSC analysis reported in Fig. S3 and S4 [16,17]. The undulations occurring in the temperature range 50–100 °C are sharp only for the iPP-LS rich blend 10/90 (Fig. 2A'), whereas for the other blends they show up as a weak waving (Fig. 2B',C').

It is worth noting that the sudden drops/rises of I_{max} marking the melting/crystallization of the two components are preceded by a significant increase/decrease of the SAXS signal with increase/decrease of the temperature. This behavior reflects the phase changes occurring at lamellar length scale in the blends and are better discussed in terms of the changes of the scattering invariant, Q, defined as:

$$Q = \frac{1}{2\pi^2}\int_0^\infty (I - I_{back}) q^2 dq \quad (1)$$

where I_{back} is the background intensity. Eq. (1) defines the total scattered intensity from an isotropic sample, after integration over the whole reciprocal space. In practice, as the scattered intensity is collected only over a limited range of q for each temperature, the integration in Eq. (1) was performed only over the sampled region comprised between $q_{min} = 0.15\ nm^{-1}$ and $q_{max} = 2\ nm^{-1}$, obtaining the reduced quantity $Q(T)$ as a function of the temperature. This quantity still holds the relevant structural information. More precisely, for each sample, the phase changes are probed by calculating from the reduced invariant $Q(T)$ the fractional invariant $R(T)$ as:

$$R(T) = \frac{Q(T) - Q_{min}}{Q_{max} - Q_{min}} \quad (2)$$

with Q_{min} and Q_{max} the minimum and maximum values, respectively, achieved by $Q(T)$.

The values the fractional invariant of the iPP-HS/iPP-LS blends with composition 90/10, 50/50 and 10/90 and for iPP-LS pure component are reported in Fig. 3 and S4, respectively, as a function of the temperature, as an example.

For the 10/90 iPP-HS/iPP-LS blend (Fig. 3A), during the heating step, the fractional invariant, after a slight increase in the temperature range 20–60 °C, shows a reduction at 70 and 150 °C, marking the melting of the low and high stereoregular components, respectively. The changes of $R(T)$ during the cooling step consist in an initial gradual

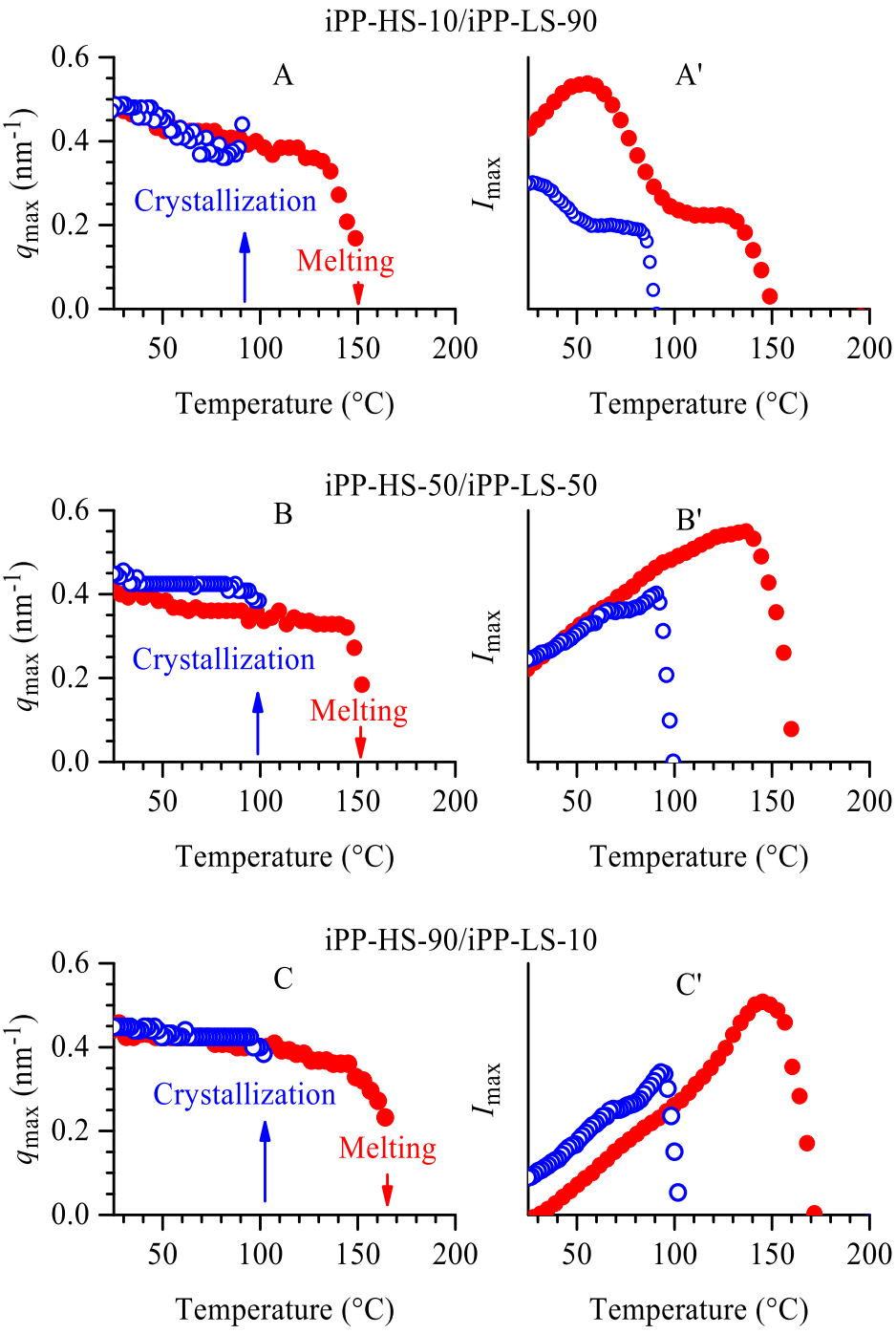

Fig. 2. Position q_{max} (A–C) and intensity value I_{max} (A′-C′) of the correlation peak in the SAXS profiles of iPP-HS/iPP-LS blends at composition 10/90 (A, A′), 50/50 (B,B′) and 90/10 (C/C′) recorded in situ during the heating step at 20 °C/min (filled circles) and the successive cooling step at 10 °C/min (open circles). In A-C the vertical arrows indicate the temperature where a peak in the scattering curve is first (crystallization) or last (melting) observed, so its position and intensity could be evaluated or not, respectively.

decrease, followed by stepwise rises at ≈80 and 40 °C due to the separate crystallization of the two components. In particular, during the heating, the sudden drop of the fractional invariant at 20–60 °C reflects well the behavior of the neat iPP-LS component upon melting (Fig. S4A). However, during the cooling, compared with the crystallization behavior of the iPP-LS component, in the 10/90 iPP-HS/iPP-LS blend (Fig. 3A), the crystallization of the pure iPP-LS sample is marked by a less pronounced increase of the fractional invariant (Fig. S2A). As discussed in ref. 17, this difference may be ascribed to the nucleating effect that the crystals of the iPP-HS component formed at high temperatures may have on the crystallization behavior of the iPP-LS component in the blends. On the other hand, for the 50/50 and 90/10 iPP-HS/iPP-LS blends (Fig. 3B and C), the fractional invariant shows a steady increase before the sudden drop at ≈ 150–170 °C due the melting of the high stereoregular component. During the cooling step, crystallization of the iPP-HS component is marked by a sudden rise at ≈80–100 °C, followed by a steady decrease toward low temperatures. In other terms, only for the blend iPP-HS/iPP-LS 10/90 the separated melting/crystallization of iPP-LS and iPP-HS at around 80 and 150 °C during heating and 40 and 80 °C during cooling appears sharp (Fig. 2A' and 3A). For the blends 50/50 and 90/10 (Fig. 2B',C′ and 3B,C), instead, the independent melting/crystallization processes of the iPP-LS component is not well-resolved, as it involves continuous changes. The temperatures of the leading melting/crystallization processes associated with the heating/cooling of the blends, may be better evidenced in the first derivative traces of the fractional invariant (Fig. 3A'-C′). Indeed, the first derivative traces show abrupt changes of $R(T)$ giving rise to peaks at temperatures close to the melting and crystallization of the iPP components derived from DSC

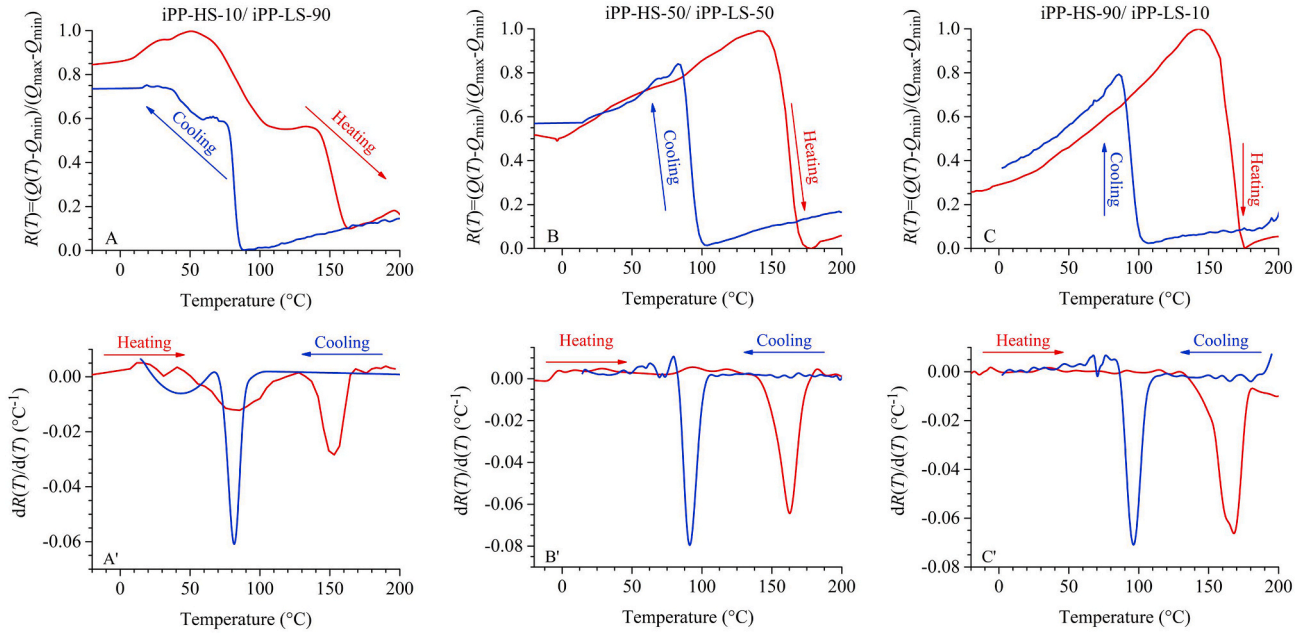

Fig. 3. Fractional scattering invariant ($R(T)$) (A–C) and first derivative of $R(T)$ with respect the temperature (A′-C′) extracted from the SAXS profiles of iPP-HS/iPP-LS blends at composition 10/90 (A,A′), 50/50 (B,B′) and 90/10 (C/C′) recorded in situ during the heating step at 20 °C/min and the successive cooling step at 10 °C/min as indicated by the direction of the arrows.

traces (Fig. S3 and S4). In particular, in agreement with the DSC thermograms of Fig. S3 and those reported in Refs. [16,17], the first derivative of the fractional invariant $R(T)$ shows pronounced melting and crystallization peaks in the temperature ranges 150–160 °C and 80–90 °C, respectively, for the iPP-HS component whereas, for the low stereoregular iPP-LS component, these peaks are less distinguishable. Only for the blends with iPP-LS content higher than or equal to 90 wt%, some broad peaks emerge at 80 °C during heating, and in the temperature range 30–40 °C during cooling (Fig. 3A'-C′, S2A′ and S4). Comparing the thermal behavior of the blends as studied with DSC and SAXS techniques, it appears that the melting and crystallization temperatures of the iPP-HS component extracted from SAXS analysis are slightly higher and lower, respectively, than those extracted from DSC analysis (Fig. 3A'-C′, S3 and S4). Moreover, the melting and crystallization peaks of the iPP-LS component extracted from SAXS analysis are less pronounced than those observed in the DSC thermograms. These differences are due to differences in the adopted heating rates (viz. 10 °C/min for DSC and 20 °C/min for SAXS measurements) and to the different sensitivity of the SAXS and DSC techniques to the structural rearrangements occurring during melting/crystallization. However, compared with the pure components, both techniques indicate that, in the blends, a small decrease of the melting temperature of the iPP-HS occurs with increase the iPP-LS content and that, for the iPP-LS component, the main melting temperature is almost invariant whereas the crystallization temperature shows a neat increase. According to Refs. [16,17], the small or negligible melting point depression of iPP-HS and iPP-LS components is due to the fact that, under identical crystallizing conditions, the thicknesses of the lamellar crystals which develop in the blends are almost identical to those which develop in the pure sample. A further reason may be also envisaged in the fact that the chemical potentials of the iPP-HS and iPP-LS chains in the blends are not greatly different from those of the neat samples, owing to the weak reciprocal interactions and hence to the good degree of miscibility of the two components in the melt and amorphous state [16,17]. The neat increase of crystallization temperature of iPP-LS component in the blends, instead, can be ascribed to the nucleating efficiency of the iPP-HS crystals on its crystallization.

It is worth noting that during heating (cooling) the value of fractional invariant (and I_{max}, Fig. 2A'-C′) increases (decreases) not only at temperatures preceding (following) a steep drop (rise), but also after complete melting (before the crystallization onset) of the high stereoregular component. The increase (decrease) of the fractional invariant (and of I_{max}) during the heating (cooling) in the melt is essentially due to an increase (decrease) of thermal fluctuations in electron density by effect of the temperature. However, the fact that the fractional invariant (and I_{max}) increases (decreases) during heating (cooling) even before complete melting of the two components, on the low temperature side, can be also due to other contributions, associated with the tendency of the two components to form different population of mixed lamellar stacks [16], with differences in the thermal expansion (dilation) coefficients of the crystalline and amorphous phases and/or to the possible occurrence of melting/recrystallization phenomena during heating as indicated by the wavy behavior of the fractional invariant of the pure iPP-LS sample (Fig. S2). A model of the mixed lamellar stacks that form in the iPP-blends upon crystallization is shown in Fig. 4A. As studied in Ref. 16, thick lamellar crystals of the iPP-HS component are mixed with thin lamellar crystals of the low stereoregular component iPP-LS in the same stacks. The low stereoregular component, in particular, forms lamellar crystals of different thickness centered around two leading values, melting at well separated temperatures of ≈55 and ≈ 88 °C, both in the neat sample and in the blends [16,17]. The lamellar crystals in the stacks are separated by amorphous layers of the intermixed coils of the two components (Fig. 4A).

In the hypothesis that the complex molecular arrangement of the iPP chains in the blends consists of mixed lamellar crystals of the two components organized in different populations of stacks [16] (average lamellar thickness/stack $<l_{ci}>$, average periodicity/stack $<L_i>$), the fractional invariant $R(T)$ may be assumed proportional to the quantity:

$$R(T) \propto \sum_{i=1}^{n} v_i \, \varphi_{ci}(1-\varphi_{ci}) + F(T) \qquad (3)$$

where v_i is the fractional amount of stacks of kind i times the contrast $(\rho_{ci}-\rho_{ai})^2$, ρ_{ci} and ρ_{ai} are the average electron density of crystalline and amorphous phases in the stack i, $\varphi_{ci} = <l_{ci}>/<L_i>$ is the corresponding linear crystallinity index, and $F(T)$ is the contribution to the invariant

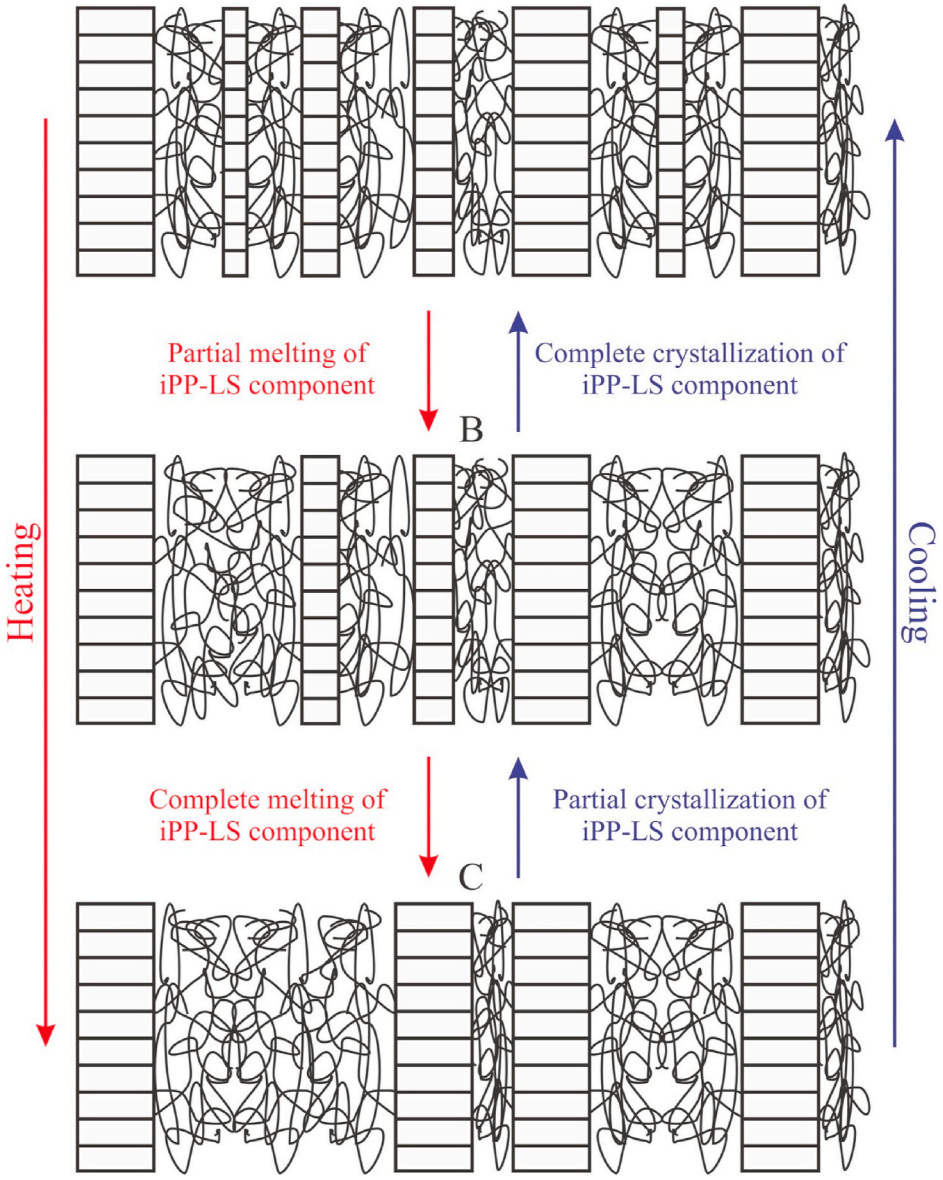

Fig. 4. Model of stacked lamellar crystals of the iPP-HS (thick crystals) and iPP-LS (thin crystals) crystals that take place in iPP-HS/iPP-LS blends (A), and successive evolution during heating/cooling leading to the gradual melting/crystallization of the thin and defective crystals of the iPP-LS component (B,C).

from thermal electron density fluctuations, partly due also to some residual background. The summation in Equation (3) is performed over all n different populations of lamellar stacks. The total volume fraction of the crystalline phase φ_c in the blends is given by equation:

$$\varphi_c = \sum_{i=1}^{n} v_i \, \varphi_{ci} \tag{4}$$

In equation (3), a decrease/increase of the local linear crystallinity index in a stack φ_{ci} due to the partial melting/crystallization of the lamellar crystals by effect of increase/decrease of temperature, respectively, may induce either a decrease or an increase of the corresponding contribution φ_{ci} (1-φ_{ci}) to the invariant ratio $R(T)$ depending on whether the φ_{ci} value is lower or higher than 50%, respectively. Therefore, the observed increase (decrease) of the fractional invariant preceding (following) a steep drop (rise) can be interpreted as due either to the gradual melting (crystallization) of the thin lamellae belonging to the low stereoregular component, embedded in stacks with local linear crystallinity index higher than 50% (Fig. 4B and C)[16,17] and/or to occurrence of disordering (ordering) phenomena leading to an increase (decrease) of contrast, and/or to melting recrystallization phenomena occurring during heating. In other terms, for the iPP-HS rich blends, the majority of stacks have linear crystallinity index around 70%.[16,17] As shown in Fig. 4B, the partial melting (crystallization) of the thin and defective lamellar crystals of the iPP-LS component, placed in the interlamellar amorphous regions of the leading iPP-HS component, induce only a small decrease (increase) of the φ_{ci} values. As long as the φ_{ci} values remain higher than 50%, these stacks are expected to give an increasingly higher (lower) contribution to the fractional invariant during heating (cooling), because the corresponding term φ_{ci} (1-φ_{ci}) increases (decreases) with decrease (increase) of φ_{ci} (Fig. 3C). At the same time, during heating, the increase of the invariant ratio is also due to the fact that the melting of the low stereoregular component creates pools embedded in the stacks filled by completely melted chains that induce an increase of the electron density fluctuations and of the contrast, as the thermal expansion of the amorphous phase is higher than that of the crystals. Similarly, during cooling, not only the electron density contrast decreases due to thermal contraction, but also the electron density fluctuations decrease, as the crystallization of the low stereoregular component creates lamellar crystals in the interlamellar

pools of amorphous phase, which act as hurdles to the segmental motion of the chains. It is worth noting that these arguments hold also for the iPP-LS rich blends and for the blend 50/50 (Fig. 3A and B). Indeed, a small population of stacks with linear crystallinity index φ_{ci} higher than 50% (Fig. 4B) do exist also in these blends. However, the fact that a large population of stacks are characterized by φ_{ci} values lower than 50%[16,17] suggests that the increase (decrease) of electron density fluctuation with increase (decrease) of the temperature consequent to the gradual melting (crystallization) of the low stereoregular component, associated with the enhanced thermal expansion (contraction) of the amorphous phase, play the main role.

3.2. Melt analysis

It is worth noting that the results of the present analysis provide definitive evidences about the tendency of the low and high stereoregular iPP samples to crystallize forming different populations of intermixed lamellar stacks in their blends. The formation of intermixed lamellar stacks strongly suggests the hypothesis that the two components show a good level of miscibility in the melt. Accordingly, phase separation is induced by the separate crystallization of the two components. In particular, the crystallization of the high stereoregular component iPP-HS at high temperature, enriches the surrounding environment of the low stereoregular sample iPP-LS. At lower temperatures, the low stereoregular component crystallizes forming lamellar crystals that partly remain entrapped in the interlamellar amorphous regions of the high stereoregular component, partly give rise to new populations of stacks in which the defective portions of chains of the high stereoregular component are either included in the crystals of the iPP-LS component, or form independent crystals embedded in the stacks. According to this scenario, the possible occurrence of a phase separation already in the melt is investigated, from the analysis of the SAXS curves collected in the melt.

The SAXS curves of the iPP-HS/iPP-LS blends at 10/90, 50/50 and 90/10 composition collected at high temperatures are reported in Fig. 5,

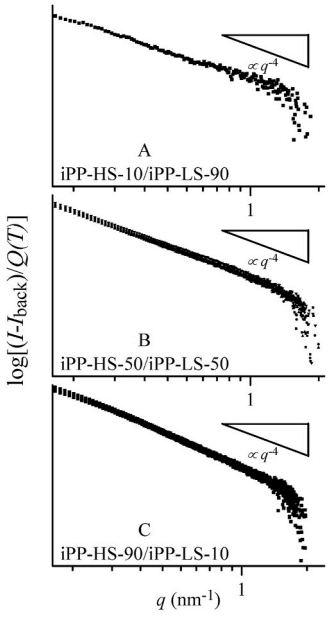

Fig. 5. SAXS curves of iPP-HS/iPP-LS blends at 10/90 (A), 50/50 (B) and 90/10 (C) composition recorded in situ during the heating step at 20 °C/min for temperatures higher than 175 °C and the successive cooling step at 10 °C/min, for temperatures higher than 120 °C. The scaling of the tails with q^{-4} is indicated. The SAXS intensity, after accurate subtraction for the background intensity has been normalized to the corresponding (reduced) invariant defined in the main text.

as an example. Data collected at 175, 190, 200 °C during heating and 150 °C during the successive cooling are reported. For each sample, the SAXS data, after subtraction for the residual background and division by the value of the corresponding reduced invariant $Q(T)$ as defined before, collapse into a single curve.

Due to the low contrast in electron density of the two components, the SAXS profiles cannot be analyzed in terms of the Random Phase Approximation (RPA) devised by de Gennes [58,59]. The RPA is a mean field approximation that neglects contributions from thermal composition fluctuations and only the spatial composition fluctuations are accounted for, in the assumption of ideal Gaussian statistics for the conformations of the chains [52,53]. According to the RPA, in a single-phase incompressible polymer blends, the scattering intensity $I(q)$ scales as q^{-2}. However, for the iPP-HS/iPP-LS blends the scattering intensity in the melt decreases with a power law of q with exponent equal to −4 (Fig. 5). This suggests that X-rays probe the thermal composition fluctuations normally observed in homogeneous polymer melts and/or the presence of nanometric impurities separated from the surrounding melt by a sharp interface.

Therefore, in order to evaluate the average correlation distance ξ over which the electron density fluctuations can be considered not to change significantly, the SAXS data of the blends in the melt state are analyzed using the Debye-Bueche (DB) equation [60]. The electron density fluctuation in a given point i, η_i is defined as the difference between the corresponding electron density ρ_i and the average electron density $<\rho>$, that is $\eta_i = \rho_i - <\rho>$. The DB equation may be applied to isotropic systems in which the normalized (auto)correlation function of electron density fluctuations $\gamma(r) = <\eta_i\eta_{j>\,r}/<\eta^2>$, with i and j two points at distance *r,* may be assumed to decay according an exponential function:

$$\gamma(r) = exp(-r/\xi) \tag{5}$$

In Equation (5) the average correlation distance ξ represents also a measure of the size of the fluctuations as well as of the extension of the inhomogeneities in the melt. The DB equation corresponds to the Fourier Transform of Equation (5) [60] and is given by:

$$I_{DB}(q) = \frac{K}{(1+q^2\xi^2)^2} \tag{6}$$

where K is a constant which places the intensity on an arbitrary scale.

As an example, and without loss of generality, the values of the inverse square root of the SAXS data collected at 175 °C for all blends (after normalization for the corresponding invariant, $(Q(T)/I)^{-0.5}$) are reported in Fig. 6 as a function of q^2 (DB plot). Similar plots would be obtained using the SAXS data collected in the melt at different temperatures.

From Fig. 6, it is apparent that all samples show a linear dependence of the quantity $(Q(T)/I)^{-0.5}$ from q^2 in almost the same q range. However, the SAXS data for the blends with iPP-HS content >50 wt% (Fig. 6B) show a slightly different slope with respect to the data of the blends with iPP-HS content ≤50 wt% (Fig. 6A). Deviations from linearity in the DB plot occur at q higher than ≈1 nm^{-1} due to the spreading of SAXS data, and at q lower than a critical value q^* equal to ≈0.4 nm^{-1} for the sample iPP-LS and the blends with iPP-HS content ≤50% (Fig. 6A'), and to q^*≈ 0.3 nm^{-1} for the sample iPP-HS and the blends with iPP-HS content >50% (Fig. 6B'). The values of the average correlation distance ξ extracted from the fit of the DB equation to the SAXS data collected at 175 °C correspond to ≈4 and ≈ 3 nm for the blends with iPP-HS content >50 wt% and ≤50%, respectively, and are similar to the correlation distance ξ obtained for the neat components iPP-LS and iPP-HS, respectively. The results obtained using the SAXS data collected in the melt at temperatures different from 175 °C are similar.

The present analysis suggests that the melt state of the iPP blends is dominated by the low strereoregular component iPP-LS for the blends with iPP-HS content ≤50%, by the high stereoregular component iPP-HS

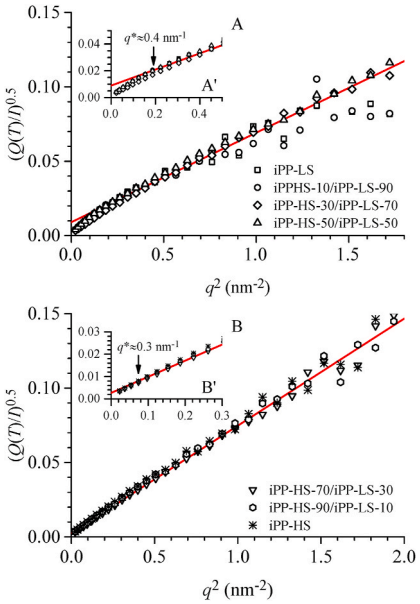

Fig. 6. Debye-Bueche plot where the square root of the ratio between the reduced invariant $Q(T)$ and the SAXS intensity I of the iPP-LS and iPP-HS samples and the corresponding blends is reported as a function of q^2. SAXS data are collected at 175 °C, for the pure iPP-LS sample and the iPP-HS/iPP-LS blends at composition 10/90, 30/70 and 50/50 (A) and for the pure iPP-HS sample and the iPP-HS/iPP-LS blends at composition 70/30, 90/10 (B). The fit of the square root of the inverse of Equation (6) to the data is indicated. Insets A′ and B′ mark the cross over occurring at q^* between the linear behavior and the curvature of the experimental data occurring in the low q region.

for the blends with iPP-HS content >50 wt%. The iPP components are largely miscible and form an entangled intermixed network in the melt. Similar to the pure components, in the melt, fluctuations of electron density occur at length scale of ≈3 nm for the blends rich in iPP-LS component and ≈4 nm for the blends rich in the iPP-HS component, giving rise to spatially correlated inhomogeneities over domains of limiting size $D = 2\pi/q^*$ equal to ≈15 and ≈ 21 nm, respectively. The size of the inhomogeneities and the size of the global domains over which fluctuations are correlated reflect the strength of the correlations, which in turn depends on the intrinsic flexibility of the chains of the leading component. For the low stereoregular sample iPP-LS and the iPP-LS rich blends, the strength of these correlations is lower than the correlation strength involved for the electron density fluctuations in the high stereoregular component iPP-HS and the iPP-HS rich blends. We infer that these differences reflect well the lower intrinsic flexibility of the chains of the low stereoregular sample iPP-LS compared with that of the high stereoregular sample iPP-HS [61].

3.3. Morphological considerations

The formation of intermixed lamellar stacks along with the melt analysis of the iPP blends strongly support the hypothesis that crystallization of the blends starts occurring from a homogeneous melt. This hypothesis is in good agreement with the homogeneous spherulitic morphologies which develop from the melt. As an example, the spherulitic morphology which develops in iPP-HS/iPP-LS blends at 10/90, 50/50 and 90/10 compositions are shown in Fig. 7. The POM images are collected at 121 °C while cooling the melt from 200 °C to room temperature at rate of 1 °C/min. At this temperature, only the high stereoregular component iPP-HS crystallizes.

For the iPP-HS/iPP-LS blend at 10/90 composition, sporadic birefringent lamellar aggregates, uniformly distributed over the whole observation area are embedded in the matrix of the low stereoregular component still in the melt state (Fig. 7A). For the iPP-HS/iPP-LS blend

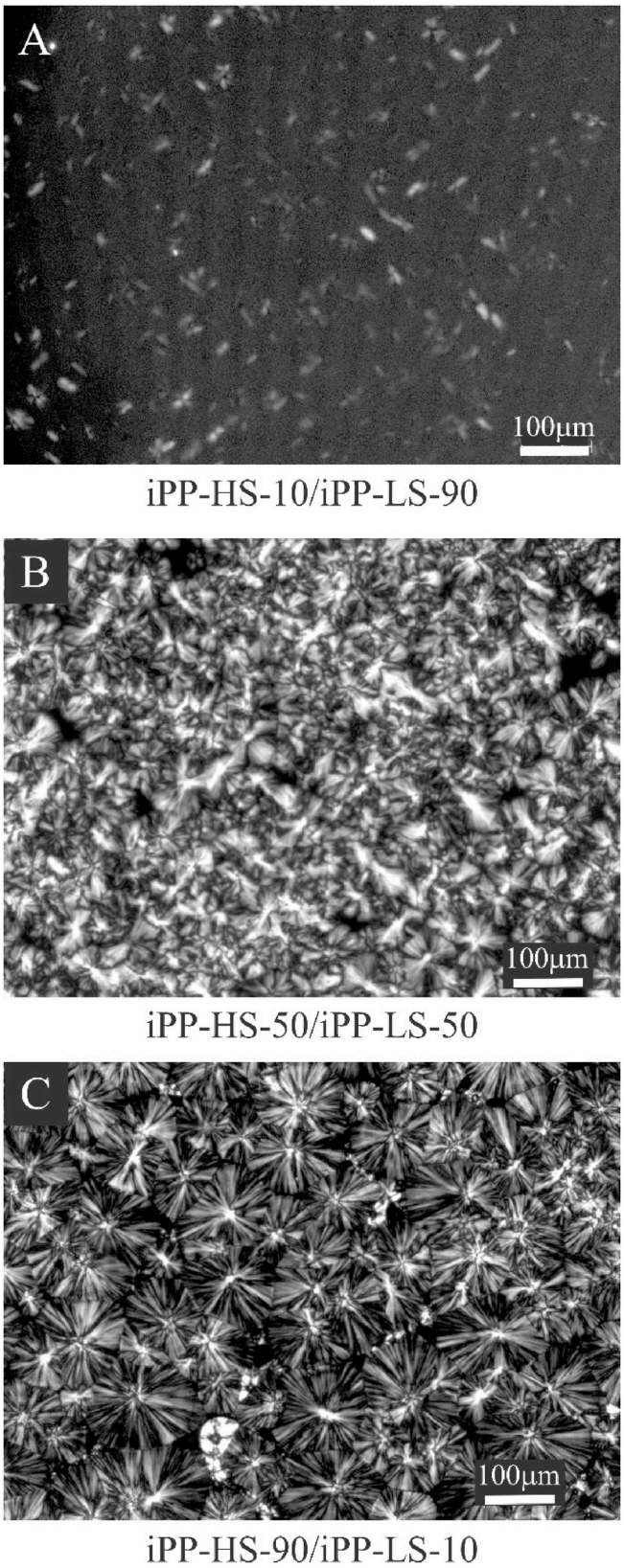

Fig. 7. Polarized optical microscopy (POM) images of iPP-HS/iPP-LS blends at 10/90 (A), 50/50 (B) and 90/10 composition. The images are recorded at 121 °C while cooling the melt from 200 °C at rate of 1 °C/min.

at 50/50 composition, the observation area is fully covered by birefringent entities of irregular shape due to the crystallization of the iPP-HS component (Fig. 7B). For the iPP-HS/iPP-LS blend at 90/10 composition, open spherulites of the iPP-HS component are formed, which assume a characteristic star-like shape, where filamentous birefringent entities emanate from a central point (Fig. 7C). The POM images of the blends in Fig. 7 are completely different from the more conventional spherulitic morphology which develops in the neat iPP-HS sample at 121 °C, under the same crystallizing condition (Fig. S5). These results indicate that the presence of even small amounts of iPP-LS component in the blends has a strong influence on the spherulitic morphology of the high stereoregular sample iPP-HS, due to the good level of miscibility of the two components in the melt.

4. Conclusions

The melting and crystallization process of blends formed by two isotactic pseudo-copolymers is investigated for the changes occurring at lamellar length scale, by performing in situ time-resolved SAXS measurements during a heating and cooling step, at a controlled scanning rate. A method for the analysis of SAXS data is devised, which demonstrates that non-trivial structural and mechanistic information may be obtained without resorting to more sophisticated experiments, based on SANS technique and deuterium labelling of polymers.

The iPP samples are characterized by a low and high degree of stereoregularity and show melting and crystallization in well separated temperature ranges. In particular, the melting temperatures of the high and low stereoregular samples occur at ≈160 and ≈ 50–90 °C, respectively, whereas the corresponding crystallization temperatures are around 117 °C and 32 °C, respectively. As the two iPP samples show the separate crystallization and melting in the blends, the present analysis has allowed to single out the leading transformations of each component in the blends as a function of temperature.

The analysis of SAXS data collected during the heating/cooling scans indicate that the two components crystallize forming different populations of intermixed lamellar stacks in the blends, due to a good level of miscibility of the corresponding chains in the melt. The formation of this complex morphology is possibly triggered by phase separation occurring in the homogeneous melt at the onset of crystallization of the high stereoregular component, according to a simple pathway. The key steps of this pathway include the progressive formation of lamellar crystals from the high stereoregular component at high temperatures, with the consequent increase of concentration of the low stereoregular component in the surrounding melted regions. Successively, mixed lamellar stacks are formed with further decrease of the temperature, as also the low stereoregular component crystallizes. The resultant lamellar crystals in part are formed within the interlamellar amorphous regions of the previously formed stacks, in part generate independent populations of stacks, possibly including the defective crystals of the high stereoregular component.

The SAXS analysis is extended to the melt. It is shown that after suitable scaling, the SAXS data of the blends collapse into unique trends, allowing to identify two subsets of blends, which behave in the melt similar to the neat components. The two subsets of blends are characterized by a different length scale of electron density fluctuations, that is by a characteristic distance for the decay of electron density fluctuations ξ of the order 3 and 4 nm for the blends rich in the low and the high stereoregular components, respectively. It is also shown that these fluctuations give rise to spatially correlated inhomogeneities over domains of limiting size of $D \approx 15$ and ≈ 21 nm, in the two subsets of blends, namely those rich in the low and the high stereoregular component, respectively. The concept of fluctuation strength is introduced, as a link to the molecular microstructure of the iPP chains. The concept entails that for the polymer blends rich in the low stereoregular component and the neat iPP-LS sample, low values of ξ and D are associated with a low correlation strength and hence with a high intrinsic flexibility of the dominant chains, whereas for the polymer blends rich in the high stereoregular component and the neat iPP-HS sample high values of ξ and D are associated with a high correlation strength and hence with a low intrinsic flexibility of the dominant chains.

Declaration of competing interest

The authors declare that they have no known competing financial interests or personal relationships that could have appeared to influence the work reported in this paper.

Acknowledgment

The Centro Ricerche Giulio Natta of LyondellBasell in Ferrara is acknowledged for the financial support. The time resolved SAXS measurements were performed at the SFTC SRS at Daresbury UK and we thank beamline staff for their assistance in performing the experiments. The work of GRM is supported by the Fundação para a Ciência e a Tecnologia (FCT) and Centro2020 through the Project references: UID/Multi/04044/2019.

Appendix A. Supplementary data

Supplementary data to this article can be found online at https://doi.org/10.1016/j.polymer.2021.123411.

References

[1] D. Jenkins, P. Kratochvíl, R.F.T. Stepto, U.W. Suter, Glossary of basic terms in polymer science (IUPAC Recommendations 1996), Pure Appl. Chem. 68 (1996) 2287–2311, https://doi.org/10.1351/pac199668122287.
[2] G. Gorrasi, V. Vittoria, P. Longo, Transport and mechanical properties of iPP–sPP fibers, J. Appl. Polym. Sci. 80 (2001) 539, https://doi.org/10.1002/1097-4628(20010425)80:4<539::AID-APP1128>3.0.CO;2-3.
[3] R. Thomann, J. Kressler, S. Setz, C. Wang, R. Mülhaupt, Morphology and phase behaviour of blends of syndiotactic and isotactic polypropylene: 1. X-ray scattering, light microscopy, atomic force microscopy, and scanning electron microscopy, Polymer 37 (1996) 2627, https://doi.org/10.1016/0032-3861(96)87621-X.
[4] R. Thomann, J. Kressler, B. Rudolf, R. Mülhaupt, Morphology and phase behaviour of blends of syndiotactic and isotactic polypropylene: differential scanning calorimetry, light transmission measurements, and PVT measurements, Polymer 37 (1996) 2635, https://doi.org/10.1016/0032-3861(96)87622-1.
[5] Z.G. Wang, R.A. Phillips, B.S. Hsiao, Morphology development during isothermal crystallization. II. Isotactic and syndiotactic polypropylene blends, J. Polym. Sci., Part B: Polym. Phys. 39 (2001) 1876, https://doi.org/10.1002/polb.1162.
[6] L. Garnier, S. Duquesne, S. Bourbigot, R. Delobel, Non-isothermal crystallization kinetics of iPP/sPP blends, Thermochim. Acta 481 (2009) 32–45, https://doi.org/10.1016/j.tca.2008.10.006, 10.1016/j.tca.2008.10.006.
[7] X. Zhang, Y. Zhao, Z. Wang, C. o Zheng, X. Dong, Z. Su, P. Sun, D. Wang, C.C. Han, D. Xu, Morphology and mechanical behavior of isotactic polypropylene (iPP)/syndiotactic polypropylene (sPP) blends and fibers, Polymer 46 (2005) 5956–5965, https://doi.org/10.1016/j.polymer.2005.05.004.
[8] D. Nwabunma, T. Kyu, Polyolefin Blends, Wiley-Interscience, Hoboken, NJ, 2008.
[9] T. Shiomura, N. Uchikawa, T. Asanuma, R. Sugimoto, I. Fujio, S. Kimura, S. Harima, M. Akiyama, M. Kohno, N. Inoue, in: J. Scheirs, W. Kaminsky (Eds.), Metallocene Based Polyolefins: Preparation, Properties and Technology, vol. 1, John Wiley & Sons, Chichester, England, 2000, pp. 437–465.
[10] R.A. Phillips, Macromorphology of polypropylene homopolymer tacticity mixtures, J. Polym. Sci., Part B: Polym. Phys. 38 (2000) 1947, https://doi.org/10.1002/1099-0488(20000801)38:15<1947::AID-POLB10>3.0.CO;2-M.
[11] Z.-G. Wang, R.A. Phillips, B.S. Hsiao, Morphology development during isothermal crystallization. I. Isotactic and atactic polypropylene blends, J. Polym. Sci., Part B: Polym. Phys. 38 (2000) 2580, https://doi.org/10.1002/1099-0488(20001001)38:19<2580::AID-POLB100>3.0.CO;2-B.
[12] R.-D. Mayer, R. Thomann, J. Kressler, R. Mulhaupt, B. Rudolf, The influence of stereoregularity on the miscibility of poly(propylene)s, J. Polym. Sci., Part B: Polym. Phys. 35 (1997) 1135, https://doi.org/10.1002/(SICI)1099-0488(199705)35:7<1135::AID-POLB12>3.0.CO;2-A.
[13] R. Silvestri, P. Sgarzi, Miscibility of polypropylenes of different stereoregularity, Polymer 39 (1998) 5871, https://doi.org/10.1016/S0032-3861(97)10247-6.
[14] J.C.W. Chien, Y. Iwamoto, M.D. Rausch, W. Wedler, H.H. Winter, Homogeneous binary zirconocenium catalyst systems for propylene polymerization. 1. Isotactic/atactic interfacial compatibilized polymers having thermoplastic elastomeric properties, Macromolecules 30 (1997) 3447, https://doi.org/10.1021/ma961726b.

[15] E.M. Woo, K.Y. Cheng, Y.-F. Chen, C.C. Su, Experimental verification on UCST phase diagrams and miscibility in binary blends of isotactic, syndiotactic, and atactic polypropylenes, Polymer 48 (2007) 5753, https://doi.org/10.1016/j.polymer.2007.07.015.
[16] F. Auriemma, O. Ruiz de Ballesteros, C. De Rosa, Theoretical investigation of nano-scale organization in blends of semicrystalline/semicrystalline polymers by small angle X-ray scattering, Macromolecules 43 (2010) 9787–9801, https://doi.org/10.1021/ma102007e.
[17] F. Auriemma, O. Ruiz de Ballesteros, C. De Rosa, C. Invigorito, Tailoring the mechanical properties of isotactic polypropylene by blending samples with different stereoregularity, Macromolecules 44 (2011) 6026–6038, https://doi.org/10.1021/ma201420f.
[18] O. Ruiz de Ballesteros, C. De Rosa, F. Auriemma, R. Di Girolamo, M. Scoti, Melting and crystallization behavior of binary blends of syndiotactic polypropylenes of different stereoregularity, Eur. Polym. J. 84 (2016) 589–601, https://doi.org/10.1016/j.eurpolymj.2016.09.034.
[19] O. Ruiz de Ballesteros, C. De Rosa, F. Auriemma, R. Di Girolamo, M. Scoti, Thermoplastic elastomers from binary blends of syndiotactic polypropylenes with different stereoregularity, Polymer 85 (2016) 114–124, https://doi.org/10.1016/j.polymer.2016.01.036.
[20] C. De Rosa, F. Auriemma, Structure and physical properties of syndiotactic polypropylene: a highly crystalline thermoplastic elastomer, Prog. Polym. Sci. 31 (2006) 145, https://doi.org/10.1016/j.progpolymsci.2005.11.002.
[21] F. Auriemma, O. Ruiz de Ballesteros, C. De Rosa, Origin of the elastic behavior of syndiotactic polypropylene, Macromolecules 34 (2001) 4485, https://doi.org/10.1021/ma002021j.
[22] C. De Rosa, M.C. Gargiulo, F. Auriemma, O. Ruiz de Ballesteros, A. Razavi, Elastic properties and polymorphic behavior of fibers of syndiotactic polypropylene at different temperatures, Macromolecules 35 (2002) 9083, https://doi.org/10.1021/ma020394+.
[23] F. Auriemma, C. De Rosa, New concepts in thermoplastic Elastomers: the case of syndiotactic polypropylene, an unconventional elastomer with high crystallinity and large modulus, J. Am. Chem. Soc. 125 (2003) 13143–13147, https://doi.org/10.1021/ja036282v.
[24] F. Auriemma, C. De Rosa, S. Esposito, G.R. Mitchell, Polymorphic superelasticity in semicrystalline polymers, Angew. Chem. Int. Ed. 46 (2007) 4325–4328, https://doi.org/10.1002/anie.200605021.
[25] K.G. Gatos, G. Kandilioti, C. Galiotis, V.G. Gregoriou, Mechanically and thermally induced chain conformational transformations between helical form I and trans-planar form III in syndiotactic polypropylene using FT-IR and Raman spectroscopic techniques, Polymer 45 (2004) 4453–4464, https://doi.org/10.1016/j.polymer.2004.03.095.
[26] N. Tian, R. Lv, B. Na, W. Xu, Z. Li, Molecular origin of enhanced strength in the monofilament of syndiotactic polypropylene because of annealing: a micro-FTIR study, J. Phys. Chem. B 113 (2009) 14920–14924, https://doi.org/10.1021/jp906563y.
[27] L. Guadagno, C. D'Aniello, C. Naddeo, V. Vittoria, S.V. Meille, Influence of the initial morphology on the elasticity of oriented syndiotactic polypropylene, Macromolecules 37 (2004) 5977–5984, https://doi.org/10.1021/ma040039e.
[28] L. Guadagno, C. Naddeo, V. Vittoria, Elasticity of syndiotactic polypropylene: insights from temperature and time dependence, Eur. Polym. J. 45 (2009) 2192–2201, https://doi.org/10.1016/j.eurpolymj.2009.05.018.
[29] L. Guadagno, C. Naddeo, V. Vittoria Mechano-reversible physical aging of elastic oriented syndiotactic polypropylene, J. Polym. Sci., Part B: Polym. Phys. 46 (2008) 599–606, https://doi.org/10.1002/polb.21395.
[30] J. Loos, T. Schimanki, Morphology–mechanical property relations in syndiotactic polypropylene (sPP) fibers, Polym. Eng. Sci. 40 (2000) 567, https://doi.org/10.1002/pen.11187.
[31] C. D'Aniello, L. Guadagno, C. Naddeo, V. Vittoria, Elastic behaviour of oriented syndiotactic poly(propylene), Macromol. Rapid Commun. 22 (2001) 104, https://doi.org/10.1002/1521-3927(200102)22:2<104::AID-MARC104>3.0.CO;2-C.
[32] G. Parthasarathy, M.S. Sevegney, R.M. Kannan, Monitoring elasticity and orientation in syndiotactic polypropylene, Polymer 46 (2005) 6335–6346, https://doi.org/10.1016/j.polymer.2005.05.144.
[33] A. Boger, B. Heise, C. Troll, O. Marti, B. Rieger, Mechanical and temperature dependant properties, structure and phase transitions of elastic polypropylenes, Eur. Polym. J. 43 (2007) 634–643, https://doi.org/10.1016/j.eurpolymj.2006.11.003.
[34] C. De Rosa, F. Auriemma, A. Di Capua, L. Resconi, S. Guidotti, I. Camurati, I. E. Nifant'ev, I.P. Laishevtsev, Structure−Property correlations in polypropylene from metallocene Catalysts: stereodefective, regioregular isotactic polypropylene, J. Am. Chem. Soc. 126 (2004) 17040, https://doi.org/10.1021/ja045684f.
[35] C. De Rosa, F. Auriemma, O. Ruiz de Ballesteros, The role of crystals in the elasticity of semicrystalline thermoplastic elastomers, Chem. Mater. 18 (2006) 3523. https://doi-org-443.webvpn.jnu.edu.cn/10.1021/cm060398j.
[36] C. De Rosa, F. Auriemma, Single site metallorganic polymerization catalysis as a method to probe the properties of polyolefins, Polym. Chem. 2 (2011) 2155, https://doi.org/10.1039/C1PY00129A.
[37] A.L. McKnight, R.M. Waymouth, Group 4 ansa-cyclopentadienyl-amido catalysts for olefin polymerization, Chem. Rev. 98 (1998) 2587, https://doi.org/10.1021/cr940442r.
[38] G.W. Coates, Precise control of polyolefin stereochemistry using single-site metal catalysts, Chem. Rev. 100 (2000) 1223, https://doi.org/10.1021/cr990286u.
[39] K. Angermund, G. Fink, V.R. Jensen, R. Kleinschmidt, Toward quantitative prediction of stereospecificity of metallocene-based catalysts for α-olexfin polymerization, Chem. Rev. 100 (2000) 1457, https://doi.org/10.1021/cr990373m.
[40] L. Resconi, L. Cavallo, A. Fait, F. Piemontesi, Selectivity in propene polymerization with metallocene catalysts, Chem. Rev. 100 (2000) 1253, https://doi.org/10.1021/cr9804691.
[41] G. Muller, B. Rieger, Propene based thermoplastic elastomers by early and late transition metal catalysis, Prog. Polym. Sci. 27 (2002) 815, https://doi.org/10.1016/S0079-6700(01)00030-2.
[42] De Rosa, M. Scoti, R. Di Girolamo, O. Ruiz de Ballesteros, F. Auriemma, A. Malafronte, Polymorphism in polymers: a tool to tailor material's properties, Polym, Crystal 3 (2020), e10101, https://doi.org/10.1002/pcr2.10101.
[43] F. Auriemma, C. De Rosa, R. Di Girolamo, A. Malafronte, M. Scoti, G.R. Mitchell, S. Esposito, Relationship between molecular configuration and stress-induced phase transitions, in: G.R. Mitchell, Ana Tojeira (Eds.), Controlling the Morphology of Polymers: Multiple Scales of Structure and Processing, Springer, 2016, pp. 287–327.
[44] F. Auriemma, C. De Rosa, R. Di Girolamo, A. Malafronte, M. Scoti, G.R. Mitchell, S. Esposito, Time-resolving study of stress-induced transformations of isotactic polypropylene through wide angle X-ray scattering measurements, Polymers 10 (2018) 162, https://doi.org/10.3390/polym10020162.
[45] De Rosa, F. Auriemma, O. Tarallo, A. Malafronte, R. Di Girolamo, S. Esposito, F. Piemontesi, D. Liguori, G. Morini, The "nodular" α form of isotactic polypropylene: stiff and strong polypropylene with high deformability, Macromolecules 50 (2017) 5434–5446, https://doi.org/10.1021/acs.macromol.7b00787.
[46] P.J. Flory, Principles of Polymer Chemistry, Cornell University Press, Ithaca: New York, 1971.
[47] P.G. deGennes, Scaling Concepts in Polymer Physics, Cornell University Press, Ithaca, New York, 1979.
[48] L.A. Utracki, Polymer Alloys and Blends, Hanser, München, 1989.
[49] K. Binder, Phase transitions in polymer blends and block copolymer melts: some recent developments, Adv. Polym. Sci. 112 (1994) 181. http://doi-org-443.webvpn.fjmu.edu.cn/10.1007/BFb0017984.
[50] K. Mortensen Schwahn, Thermal composition fluctuations in polymer blends studied with small angle neutron scattering, in: W. Brown, K. Mortensen (Eds.), Scattering in Polymeric and Colloidal Systems, Gordon & Breach Science Publishers, Amsterdam, 2000.
[51] Schwahn, Critical to mean field crossover in polymer blends, Adv. Polym. Sci. 183 (2005) 1, https://doi.org/10.1007/b135882.
[52] J.S. Higgins, H. Benoit, Polymers and Neutron Scattering, Clarendon Press, Oxford, 1994.
[53] R.J. Roe, Methods of X-Ray and Neutron Scattering in Polymer Science, Oxford University Press, New York, Oxford, 2000.
[54] R. Mitchell, Xesa – X-ray experimental structural analysis for polymers, in: Vol 3 CDRSP Knowledge Series. Series, Geoffrey Mitchell and Paula Faria Institute Polytechnic of Leiria, 2018. ISBN 978-989–96766 (e-book).
[55] P. Maiti, M. Hikosaka, K. Yamada, A. Toda, F. Gu, Lamellar thickening in isotactic polypropylene with high tacticity crystallized at high temperature, Macromolecules 33 (2000) 9069–9075, https://doi.org/10.1021/ma000686f.
[56] M. Hikosaka, Unified theory of nucleation of folded-chain crystals and extended-chain crystals of linear-chain polymers, Polymer 28 (1987) 1257, https://doi.org/10.1016/0032-3861(87)90434-4.
[57] M. Hikosaka, Unified theory of nucleation of folded-chain crystals (FCCs) and extended-chain crystals (ECCs) of linear-chain polymers: 2. Origin of FCC and ECC, Polymer 31 (1990) 458, https://doi.org/10.1016/0032-3861(90)90385-C.
[58] P.G. de Gennes, Theory of X-ray scattering by liquid macromolecules with heavy atom labels, J. Phys. 31 (1970) 235–238, https://doi.org/10.1051/jphys:01970003102-3023500.
[59] P.G. de Gennes, Dynamics of fluctuations and spinodal decomposition in polymer blends, J. Chem. Phys. 72 (1980) 4756, https://doi.org/10.1063/1.439809.
[60] P. Debye, A.M. Bueche, Scattering by an inhomogeneous solid, J. Appl. Phys. 20 (1949) 518, https://doi.org/10.1063/1.1698419.
[61] G.R. Mitchell, B. Rosi-Schwartz, D.J. Ward, Local order in polymer glasses and melts, Phil. Trans. Roy. Soc. Lond. 348 (1994) 97–115, https://doi.org/10.1098/rsta.1994.0083.